Applied Chemical Engineering (2025) Volume 8 Issue 4 ISSN: 2578-2010 (O)
doi: 10.59429/ace.v8i4.5761

ORIGINAL RESEARCH ARTICLE

A novel hybrid reforming reactor for enhanced CO_2 conversion and hydrogen production: A CFD analysis

Ali Khalid Mohsen*, Tahseen A. Al-Hattab

University of Babylon, College of Engineering, Chemical Engineering department, Bail, Hilla, 51001, Iraq
***Corresponding author:** Ali Khalid Mohsen; eng446.ali.khalid@student.uobabylon.edu.iq

ABSTRACT

The use of hydrogen as an energy carrier has gained significant attention due to its environmentally friendly characteristics. Among various production methods, steam reforming of natural gas (CH_4) remains the most cost-effective and widely adopted technique. To enhance the efficiency and carbon utilization of this process, a novel hybrid steam and dry reforming reactor has been proposed, which utilizes the CO_2 produced from steam reforming within a dry reforming zone.

In this study, a two-dimensional axisymmetric hybrid catalytic membrane reactor (CMR) model was developed for the production of pure hydrogen from natural gas, employing a Pd–Ru metallic membrane and a carbonate dual-phase membrane, integrated with Ni/Al_2O_3 and Rh/Al_2O_3 catalysts. A computational fluid dynamics (CFD) approach was employed to investigate the reactor's performance in terms of methane conversion and hydrogen production under various operating conditions. These include reaction temperatures of 700, 800, 900, and 1000 K, a gas hourly space velocity (GHSV) of 1000 h^{-1}, and a sweep gas Reynolds number (Re) of 100.

Simulation results revealed that the CMR achieved a high hydrogen permeation rate on the permeate (tube) side, along with a maximum CH_4 conversion of approximately 99.9% at 1000 K on the retentate side within the steam reforming zone. Furthermore, the reactor demonstrated effective syngas production with near-complete CO_2 reduction on the dry reforming side, where CO_2 concentrations at the reactor outlet approached zero at 1000 K. These findings highlight the promising potential of the hybrid combined membrane reactor (CMR) system for efficient hydrogen production and near-complete carbon utilization.

Keywords: Methane reforming; H2 production; Pd-Ru membrane; carbonate dual-phase membrane; CO2 utilization

ARTICLE INFO

Received: 2 September 2025
Accepted: 25 September 2025
Available online: 10 October 2025

1. Introduction

The increasing global demand for energy, combined with the environmental impacts of fossil fuel consumption, has created an urgent need for renewable and cleaner energy sources. In this context, hydrogen is considered one of the most promising alternatives due to its high energy density and zero direct emissions [1].

While hydrogen can be produced through various methods, the majority is currently generated from fossil fuel reforming processes [2].

Among the several pathways for syngas production from methane, methane steam reforming (SMR), methane dry reforming (DMR), and partial oxidation (PO) are the primary routes, differing in their oxidizing agents—water, carbon dioxide (CO_2), or oxygen—and operating temperatures. The combination of two or more of SMR, DMR, and PO has been the research interests form many researchers

as they have the- ability to take the benefits and reduce drawbacks concerning each of the three main routes [11].

Methane steam reforming (SMR) is the most widely employed method for hydrogen production due to its high hydrogen yield and the ready availability of fossil fuels [3].

However, the process is highly endothermic, requiring substantial external energy input to convert methane into syngas [4], which highlights the need for more efficient or integrated reforming approaches.

For a high methane conversion to occur, a steam reforming process normally accomplished on a catalyst with temperature around 800 °C or more because of the endothermic behavior of the reaction, and it's normally happened with a water gas shift reaction which increases the hydrogen yield [5].

In methane steam reforming, the reaction system involves a strongly endothermic reforming reaction, accompanied by a moderately exothermic reaction, namely the water–gas shift (WGS) reaction [6].

On the other hand, methane dry reforming is easier form the processing side than steam reforming as there is no water evaporation here, but at the same time it offers less hydrogen production [7].

In the dry reforming process methane reacts with carbon dioxide for production of hydrogen [8].

Along with dry reforming many side reactions may happen like reverse water gas shift reaction (RWGS) which will generate water [9]:

(RWGS) $CO_2 + H_2 \rightarrow CO + H_2O$ $[\Delta H^0_{298} = 41$ kJ /mol]

(WGS) $CO + H_2O \rightarrow CO_2 + H_2$ $[\Delta H^0_{298} = -41$ kJ /mol]

Another undesired reaction from catalyst deactivation side is Boudouard reaction or methane decomposition which generate carbon that accumulate on catalyst surface [10]:

(Boudouard) $2CO \rightarrow C + CO_2$ $[\Delta H^0_{298} = -171$ kJ/ mol]

(Methane decomposition) $CH_4 \rightarrow C + 2H_2$ $[\Delta H^0_{298} = 75$ kJ /mol]

Steam reforming (SMR) produces syngas with a relatively high H_2/CO ratio (3:1–5:1), whereas dry reforming (DMR) generates a lower ratio (~1:1). Integrating SMR and DMR offers the potential to produce syngas with an H_2/CO ratio suitable for Fischer–Tropsch synthesis while simultaneously consuming greenhouse gases such as CO_2 and CH_4, which is environmentally favorable [12].

Lim et al. [21] found that combined process of SMR and DMR could reduce net CO_2 emission by 67% at the optimal condition compared with the reference SMR process. By lowering the hydrogen cost less than 1.7 (US \$/kg H_2), the combined process gave lower extended mitigation cost (EMC) than the reference SMR process.

The combination of chemical reaction and separation processes is done by the catalytic membrane reactor, as a result, enhancement in compactness and efficiency is achieved. The use of catalytic membrane reactors has the ability to enhance steam methane reforming reactions performance based on Le Chatelier's principle [13].

A reactor of hybrid membrane-catalyst for production of syngas and ultrapure hydrogen which contains incantations cylinder that construct from steel that resists the heat with a cover twisted-off was developed by Fedotov et al. [14]. A porous ceramic catalytic converter has been fixed inside of the cover through a gasket of graphite with a clamping nut. A palladium-containing membrane was fixed along an outlet pipe of the membrane reactor into the inner channel of the converter which is necessary for ultrapure hydrogen selectively removal from the reaction zone.

Recently, palladium alloys with silver addition are widely used in commercial applications. As a result of their perfect permeability and total selectivity, the membranes produce ultra-pure hydrogen and will maximize the shift effect when these alloys are applied [15]. The inclusion of silver in these materials presents several issues. Above 450°C, it results in reduced hydrogen purity and the presence of oxygen. Additionally, silver-containing palladium alloys are permanently susceptible to poisoning by even minimal sulfur compounds in the gas. On the other hand, palladium alloys without silver offer superior mechanical strength, enhanced corrosion resistance, and flexibility across various operating temperatures [16].

Anzelmo et al. [23] developed a Pd-alumina composite membrane and evaluated its performance in a membrane reactor for high-purity hydrogen production via steam reforming at 420°C. Two synthetic natural gas mixtures were tested: one with N_2 alone and another with both N_2 and CO_2 to assess the effect of impurities.

Chompupun et al. [24] studied hydrogen production via steam methane reforming using a Pd membrane, combining experimental and 2D/3D computational analyses. They identified an optimal membrane design balancing hydrogen generation and permeation rate, with a recommended surface area-to-volume ratio of 255 m^2/m^3.

Nayebossadri et al. [25] investigated hydrogen separation from hydrogen–natural gas mixtures using commercial Pd, PdCu53, and PdAg24 membranes. The study focused on membrane performance under varying hydrogen concentrations, pressures, and temperatures, along with the effects of gas impurities. Among the tested membranes, PdAg24 showed superior efficiency, even at hydrogen concentrations as low as 15%. However, effective operation requires temperatures above 350 °C and a high-pressure differential.

According to Ullah et al. [28], the traditional steam methane reformer (SMR) produces ultrapure hydrogen under mild operating conditions by utilizing a hydrogen-permeable selective membrane. The researchers identified that an inlet temperature of 500 K, an operating pressure of 8.5 bar, and a gas hourly space velocity (GHSV) of 4500 hr^{-1} were critical for achieving optimal CH_4 conversion and H_2 recovery.

Combining methane steam reforming (MSR) with carbon capture and storage offers a promising route to reduce emissions in hydrogen production. Instead of relying on energy-intensive post-combustion capture, this system enables in situ CO_2 separation and recycling. The captured high-purity CO_2 can then be reinjected for methane dry reforming, forming a novel CO_2-reinjection-driven hydrogen production process [29].

The combined steam–dry reforming approach has gained significant attention as a sustainable pathway for hydrogen and syngas production, as it enables efficient utilization of greenhouse gases and provides operational flexibility for downstream applications [30].

Gangadharan et al. [26] simulated both SMR and SMR+DRM processes, evaluating their economic and environmental performance. Their analysis showed that the SMR+DRM process offers a lower carbon footprint. They suggested that advancements in DRM catalysts could improve its economic viability, making it a strong alternative to conventional SMR.

A modern design concept for reforming reactor was proposed for utilization of carbon dioxide (CO_2) generated in the methane steam reforming by implementing a catalyst filled in CO_2 separation membrane for dry reforming, connected SMR and DMR. The CO_2 produced in steam methane reforming would be selected by the membrane and would be consumed as a reactant for dry reforming inside membrane. Permeated CO_2 would react with methane for syngas production, H_2 and CO. The methane conversion achieved in this study was relatively low [17].

Shakouri et al. [31] demonstrated that combined steam and dry methane reforming over Ni and Co catalysts can enhance CO_2 conversion and allow control of the H_2/CO ratio. This hybrid approach provides a more efficient and flexible route for hydrogen and syngas production compared to individual reforming methods.

J. Lee et al. [27] introduced an innovative reactor design combining steam and dry reforming, aimed at adjusting the H_2/CO ratio and minimizing coking. Their approach uses a structured catalyst packing of inert material, followed by dry and steam reforming catalyst layers. This configuration promotes immediate CO_2 utilization, reduces coke formation due to H_2O presence, and eliminates the need for separate CO_2 removal.

A CFD modeling has become an essential tool for predicting reactor performance and designing efficient hybrid reforming systems by accounting for heat and mass transfer, catalyst activity, and reaction kinetics [32].

However, in this work, the performance of utilization of CO_2 arising from steam reforming process by dry reforming process in hybrid catalytic membrane reactor contains palladium-based membrane for H_2 permeance and carbonate dual-phase membrane for CO_2 permeance will be investigated across reaction temperatures. A 2-D axisymmetric Computational Fluid Dynamics (CFD) simulation using the software COMSOL Multiphysics 6.2 was applied. The results of (CFD) analysis are expected to provide valuable insights that guide the future development and improvement of catalytic membrane reactor design and the enhancement of hydrogen separation processes.

2. Modeling

2.1. Physical model

The 2-D axisymmetric hybrid catalytic membrane reactor is depicted in **Figure 1** the hybrid catalytic membrane reactor possesses a geometric structure characterized by a length of 500 mm.

In steam reforming side the reactor shell diameter is 20 mm, tube is 32 mm. In dry reforming the reactor side shell diameter of dry reforming is 44 mm, tube diameter of dry reforming is 64 mm.

The membranes were a dense Pd-Ru (Ru4.5%) supported on ceramic porous walls (Γ_3 & Γ_{10} in **Figure 2**) of porosity of (ε=0.5) identical to that of the catalytic bed in the permeate to ensures the continuity in CFD model [13].

The CO_2 produced in steam reforming process is passing to the dry reforming tube through a ceramic-carbonate dual-phase membrane $Ce_{0.8}Sm_{0.2}O_{1.9}$ (SDC)-carbonate dual-phase membrane (Γ_{11} in **Figure 2**) identical to that of the catalytic bed in the permeate to ensures the continuity in CFD model [18].

The membranes are arranged in a tube-shell configuration, with two distinct sides: the reforming side, also referred to as the retentate section (Ω_2 &Ω_4 in **Figure 2**), and the permeate section (Ω_1 &Ω_3 in **Figure 2**). The two sections are divided by a layer of the Pd-Ru membrane for H_2 permeation in steam and dry reforming side (Γ_3& Γ_{10} in **Figure. 2**), and the steam reforming side is separated from dry reforming side by a ceramic-carbonate dual-phase membrane for CO_2 permeation (Γ_{11} in **Figure 2**). The H_2 product exhibits the ability to permeate across the membrane and subsequently migrates towards the tubing located in the permeate sections, same time the CO_2 product exhibits the ability to permeate across the membrane and subsequently migrates towards the tubing located in the retentate section of dry reforming side. This migration process results in the generation of H_2 product, facilitated by the flow of argon sweep gas. In the retentate section of the hybrid membrane reactor, which is equipped with Ni/Al_2O_3 catalyst for steam reforming [13] and Rh/Al_2O_3 catalyst for dry reforming [19], the vacancy fraction in the bed is 0.5. During the process of reforming processes, the creation of hydrogen (H_2), carbon dioxide (CO_2), and carbon monoxide (CO) species takes place, and these species then exit by the outlet. The model and simulation incorporated both the retentate and permeate sides. **Table 1** provides a comprehensive summary of the simulation's parameters and information, encompassing various aspects such as the geometric structure of the reactor and its corresponding operating parameters.

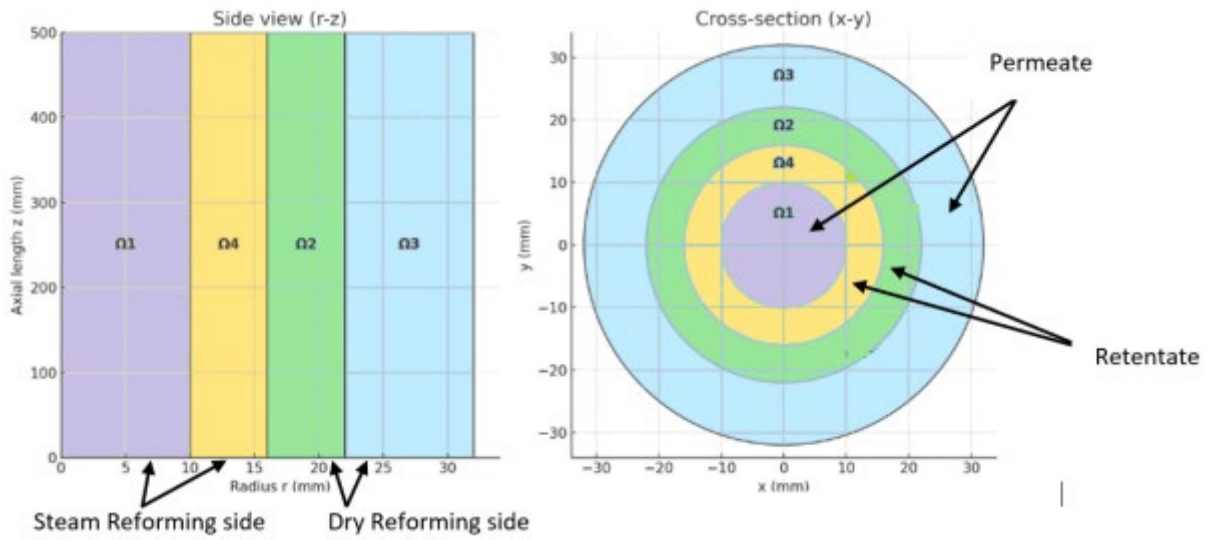

Figure 1. Hybrid Catalytic Membrane Reactor (CMR) Geometry

Table 1. System geometry and operation requirements

Description	Value
Length, mm	500
Shell diameter steam, mm	20
Tube diameter steam, mm	32
Shell diameter dry, mm	44
Tube diameter dry, mm	64
Catalyst for steam	Ni/Al_2O_3
Catalyst for dry	Rh/Al_2O_3
Porosity (ε)	0.5
H_2 selective membrane	Pd-Ru (Ru4.5%)
CO_2 selective membrane	$Ce_{0.8}Sm_{0.2}O_{1.9}$ (SDC)

2.2. Mathematical model

In order to precisely quantify the transformation of reactants (steam and methane for steam reforming, carbon dioxide and methane for dry reforming) into products (hydrogen fuel) under varying circumstances, the researchers integrated the reaction kinetics model with reactor-scale computational fluid dynamics (CFD) modeling. The inclusion of detailed transport phenomena, reaction kinetics, and the implementation of a kinetic model specific to the catalyst are outside the scope of this work. Hence, the catalyst bed was subjected to (CFD) simulation, wherein it was represented as a porous medium and modeled using a volumetric species transport model. In the current investigation, the study examines the widely accepted simplified global kinetics expressions that were previously offered by ref. [22] with catalyst Ni/Al_2O_3, and ref. [19] with catalyst Rh/Al_2O_3 are adopted.

The subsequent assumptions will aid in the construction of the mathematical model:

- The catalytic membrane reactor (CMR), steady state and non-isothermal condition.
- Neglected the effect of gravity.
- All gas mixtures as ideal gas.
- Laminar Flow in both sides and all the inlets/outlets.

- The Pd-Ru membrane is permeable only for hydrogen and ceramic-carbonate dual-phase membrane is permeable only for carbon dioxide.
- The reformer sides content catalysts, porous medium and homogeneous.
- Neglectable deactivation of catalyst by coke formation.

The following reaction equations govern the steam and dry methane gas reforming process:

Steam reforming:

1- $CH_4 + H_2O \rightarrow CO + 3H_2$ $\Delta H^0_{298} = +206$ kJ /mol. [22]

2- $CO + H_2O \rightarrow CO_2 + H_2$ $\Delta H^0_{298} = -41.15$ kJ/ mol. [22]

3- $CH_4 + 2H_2O \rightarrow CO_2 + 4\ H_2$ $\Delta H^0_{298} = 165$ kJ /mol. [22]

Dry reforming:

4- $CH_4 + CO_2 \rightarrow 2CO + 2H_2$ $\Delta H^0_{298} = 247.3$ kJ/mol. [19]

5- $CO_2 + H_2 \rightarrow CO + H_2O$ $\Delta H^0_{298} = 41.15$ kJ/mol. [19]

The rates of kinetic, constant, and equilibrium chemical reactions for reforming CH_4 with steam and CH_4 with CO_2 are shown in **Tables 2** and **3**.

Table 2. The reaction rate equations of methane steam and dry reforming

Steam Methane Reforming: 1	$r_1=\frac{k_1}{p_{H_2}^{2.5}}\left(p_{CH4}p_{H_2O}-\frac{p_{H2}^3 p_{CO}}{ke_1}\right)(DEN)^{-2}$	[22]
Water Gas Shift Reaction: 2	$r_2=\frac{k_2}{p_{H_2}}\left(p_{CO}p_{H_2O}-\frac{p_{H2}p_{CO2}}{ke_2}\right)(DEN)^{-2}$	[22]
Overall Steam Reforming reaction: 3	$r_3=\frac{k_3}{p_{H_2}^{3.5}}\left(p_{CH4}p^2{}_{H_2O}-\frac{p_{H2}^4 p_{CO2}}{ke_3}\right)(DEN)^{-2}$ $DEN = 1+ k_{CO}p_{CO} + k_{H2}p_{H2} +k_{CH4}p_{CH4} +k_{H2O}(p_{H2O}/p_{H2})$	[22]
Dry Methane Reforming: 4	$r_4=k_4(k_{CO2}\,k_{CH4}\,p_{CO2}\,p_{CH4})\ x\ (1+k_{CO2}p_{CO2}+ k_{CH4}p_{CH4})^{-2}\ x\ (1-(p_{CO}\,p_{H2})^2\ x\ (K_{e4}\,k_{CH4}\,p_{CO2})^{-1})$	[19]
Reverse Water Gas Shift reaction: 5	$r_5= k_2\,p_{CO2}(1-p_{CO}p_{H2O}\ X\ (K_{e5}\,p_{CO2}\,p_{H2})^{-1}$	[19]

Table 3. The reaction constant of natural gas steam reforming

Kinetic-constant coefficients:	**Steam reforming**	
	$k_1 = 4.22\times 10^{15}$ exp (- 240100/RT)	[22]
	$k_2 = 1.955\times 10^{6}$ exp (- 67130/RT)	[22]
	$k_3 = 1.02\times 10^{15}$ exp (- 243900/RT)	[22]
	Dry reforming	
	k_4 =1290 exp (-102065/RT)	[19]
	k_5 =1.586 exp (-73105/RT)	[19]
Equilibrium constants:	**Steam reforming**	
	$Ke_1 = 1.198\times 10^{13}$ exp (- 26830/RT)	[13]
	$Ke_2 = 1.767\times 10^{-2}$ exp(4400/RT)	[13]
	$Ke_3 = 2.117\times 10^{11}$ exp (- 22430/RT)	[13]
	Dry reforming	

	$Ke_4 = \exp(34.011) \exp(258598.7/RT)$	[19]
	$Ke_5 = (68.68) \exp(37500.7/RT)$	[19]
Adsorption constants:	**Steam reforming**	
	$k_{CH4} = 6.65\times 10^{-4} \exp(38280/RT)$	[22]
	$k_{H2O} = 1.77\times 10^{5} \exp(-88680/RT)$	[22]
	$k_{H2} = 6.12\times 10^{-9} \exp(82900/RT)$	[22]
	$k_{CO} = 8.23\times 10^{-5} \exp(70650/RT)$	[22]
Adsorption constants:	**Dry reforming**	
	$k_{CH4} = 2.60\times 10^{-2} \exp(40684/RT)$	[19]
	$k_{CO2} = 2.61\times 10^{-2} \exp(37641/RT)$	[19]

Table 3. (*Continued*)

The computational fluid dynamics (CFD) model depicted in **Figure. 2** is axisymmetric and operates in a two-dimensional (2-D) domain. The governing equations for the shell and tube sides of the Computational Fluid Dynamics (CFD) model, implemented using the COMSOL metaphysics software with the fully coupled solver, are presented in **Table 4**.

$$D_{ik}=0.0018583\sqrt{T^3\left(\frac{1}{M_i}-\frac{1}{M_k}\right)}\ \frac{1}{P\sigma_{iK}^2\Omega D_{ik}} \tag{1}$$

The estimation of the flux of H_2 through the membrane can be conducted using the Richardson equation (2):

$$J_{H_2}=p^0 e^{-\frac{E_a}{RT}}\left(P^{0.5}_{\text{retentate},H_2}-P^{0.5}_{Permeate,H_2}\right) x\ M_{w,H_2} \tag{2}$$

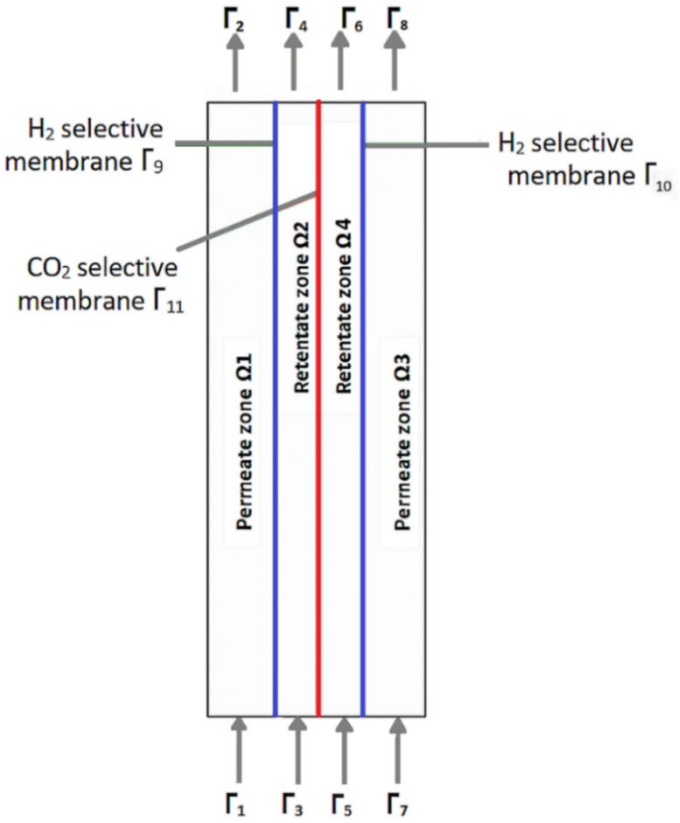

Γ_1, Γ_7: Argon sweep gas, Γ_2, Γ_8:H_2 permeate outlet, Γ_3: CH_4 and H_2O feed inlet, Γ_5: CO_2 feed inlet, Γ_4, Γ_6: retentate outlet

Figure 2. Schematic Diagram of 2-D Symmetric (Hybrid MR) Model

The rate of natural gas (methane) conversion is calculated as equation below:

$$x_i = \left(1 - \frac{F_i, exit}{Fi\, feed}\right) \times 100\% \quad (3)$$

Where F refers to normal mass flowrate and i refers to methane.

Table 4. A CFD governing equations

Retentate Side for steam and dry (Ω_2, Ω_4)	**Permeate Side for steam and dry (Ω_1, Ω_3)**
• Continuity equation: $\nabla\cdot(\varepsilon\rho\vec{v})=0$ $\rho=\frac{P}{RT\Sigma_i \frac{w_i}{Mi}}$ • Momentum equation $\vec{v}=-\frac{\kappa}{\mu}\nabla p$ • Mass equation $\nabla j_i+\rho(u\cdot\nabla)w_i=R_i$ $j_i=-\left(\rho w_i\sum_k D_{ik}d_k+D_i\frac{\nabla T}{T}\right)$ $d_k=\nabla x_k+\frac{1}{\rho_A}\left[(x_k-w_k)\nabla\rho_A\right]$ $x_k=\frac{w_k}{M_k}M_n$ $M_n=\left(\sum_i \frac{w_i}{M_i}\right)^{-1}$ • Energy equation $C_p\nabla\cdot(\rho\vec{v}\cdot T)=\nabla\cdot(k\cdot\Delta T)+\rho\sum_{i=1}^{n} r_i\Delta H_i$	• Continuity equation: $\nabla\cdot(\rho\vec{v})=0$ $\rho=\frac{P}{RT\Sigma_i \frac{w_i}{Mi}}$ • Momentum equation $\rho\vec{v}\cdot\nabla\vec{v}=\nabla\left[-IP+\mu(\nabla\vec{v})+(\nabla\vec{v})^T-\frac{2^\mu}{3}(\nabla\vec{v})\right]$ • Mass equation $\nabla j_i+\rho(u\cdot\nabla)w_i=0$ $j_i=+\left(\rho w_i\sum_k D_{ik}d_k+D_i\frac{\nabla T}{T}\right)$ $d_k=\nabla x_k+\frac{1}{\rho_A}\left[(x_k-w_k)\nabla\rho_A\right]$ $x_k=\frac{w_k}{M_k}M_n$ $M_n=\left(\sum_i \frac{w_i}{M_i}\right)^{-1}$ • Energy equation $C_p\nabla\cdot(\rho\vec{v}\cdot T)=\nabla\cdot(k\cdot\Delta T)$

2.3. Boundary conditions

The boundary conditions at inlet of the shell and tube sides are set as below:

Permeate zone of steam ref. Ω_1	**Retentate zone of steam ref. Ω_2**	**Permeate zone of dry ref. Ω_3**	**Retentate zone of dry ref. Ω_4**
$u=u_{\Gamma 1}$	$u=u_{\Gamma 3}$	$u=u_{\Gamma 7}$	$u=u_{\Gamma 5}$
$w_{Ar}=1$	$w_i=w_{i,\,\Gamma 3}$	$w_{Ar}=1$	$w_i=w_{i,\,\Gamma 5}$
$p=p_{\Gamma 2}$	$p=p_{\Gamma 4}$	$p=p_{\Gamma 8}$	$p=p_{\Gamma 6}$

At the membrane interface (Γ_9) for steam reforming:

$$-\vec{\mathbf{n}}\cdot(\mathbf{j_{H2}}+\vec{\boldsymbol{\rho}}\mathbf{w_{H2}}\vec{\mathbf{v}}) = \mathbf{P}\boldsymbol{mo}\ (\mathbf{P^{0.5}_{H2,\,\Omega 2}}-\mathbf{P^{0.5}_{H2,\,\Omega 1}})\ \mathbf{M_{H2}}\ @\ \boldsymbol{\Omega}_2$$

$$+\vec{\mathbf{n}}\cdot(\mathbf{j_{H2}}+\boldsymbol{\rho}\mathbf{w_{H2}}\vec{\mathbf{v}}) = \mathbf{P}\boldsymbol{mo}\ (\mathbf{P^{0.5}_{H2,\,\Omega 2}}-\mathbf{P^{0.5}_{H2,\,\Omega 1}})\ \mathbf{M_{H2}}\ @\ \boldsymbol{\Omega}_1$$

At the membrane interface (Γ_{10}) for dry reforming:

$$-\mathbf{n}\cdot(\mathbf{j}_{H2}+\rho\mathbf{w}_{H2}\mathbf{v}) = \boldsymbol{Pmo}\,(P^{0.5}_{H2,\,\Omega4} - P^{0.5}_{H2,\,\Omega3})\,M_{H2} \;@\; \Omega_4$$

$$+\mathbf{n}\cdot(\mathbf{j}_{H2}+\rho\mathbf{w}_{H2}\mathbf{v}) = \boldsymbol{Pmo}\,(P^{0.5}_{H2,\,\Omega4} - P^{0.5}_{H2,\,\Omega3})\,M_{H2} \;@\; \Omega_3$$

Where: $\boldsymbol{Pm}$ is the membrane permeance for H_2.

3. Results and discussion

The key parameters and their values used in this study are shown in **Table 6**. The natural gas (NG) mixture used in this study consisted of methane (CH_4), carbon dioxide (CO_2), hydrogen (H_2), carbon monoxide (CO), and water steam. The mixture flowed through the packed bed (retentate side) as the reactants. In the tube (permeate side), argon gas swept the hydrogen that permeated through the membrane.

A mesh independence study was conducted by simulating steam mole fraction profiles across the reformer bed for mesh sizes ranging from 30,000 to 140,000 elements.

As shown in **Figure 3**, the results converge after 70,000 elements with negligible variation (<0.5%). Therefore, a mesh size of 70,000 elements with a growth ratio of 1.1 was selected for the final simulations to ensure both accuracy and computational efficiency.

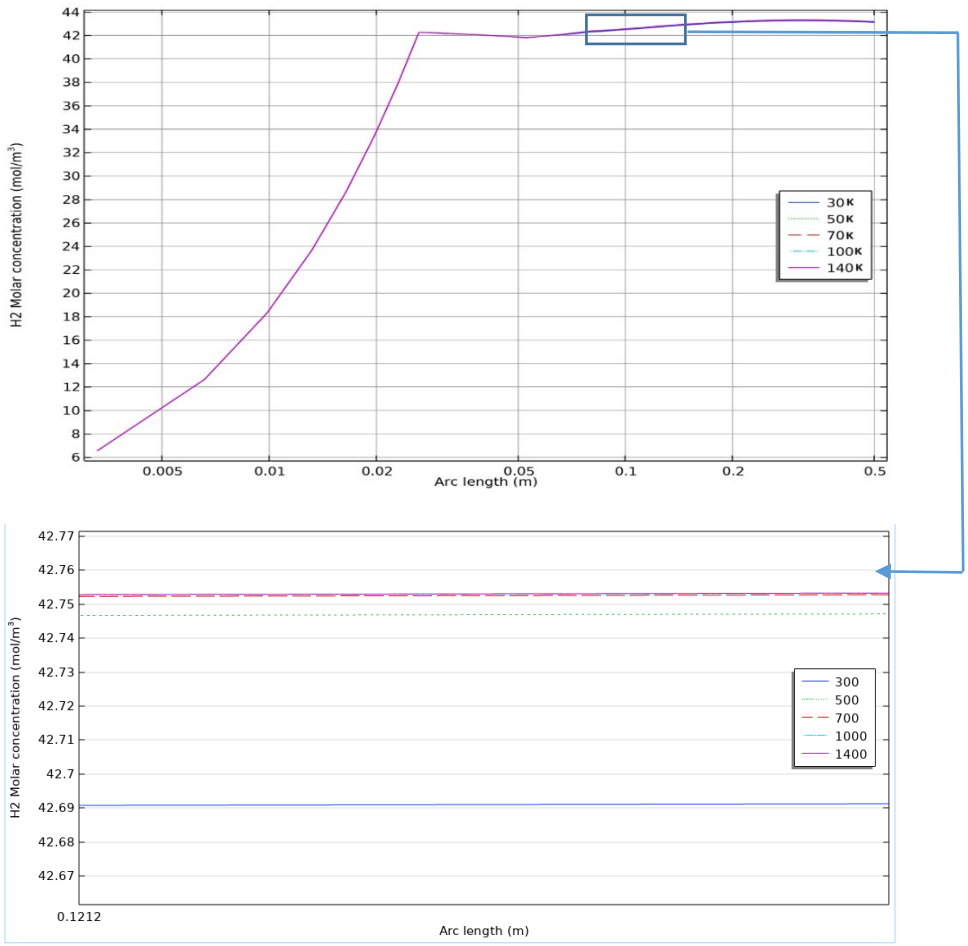

Figure 3. Grid Independence H_2 Mole Concentration Profile vs Number of Elements

Table 5. Validation difference

Membrane No.	Finer mesh (%) 5×10^{-5} kg m^{-2} s^{-1}	Finer mesh validation (%) 5×10^{-5} kg m^{-2} s^{-1}	Difference %
2	30.22	29.29	0.93
3	30.15	29.289	0.861
4	30.12	29.285	0.835

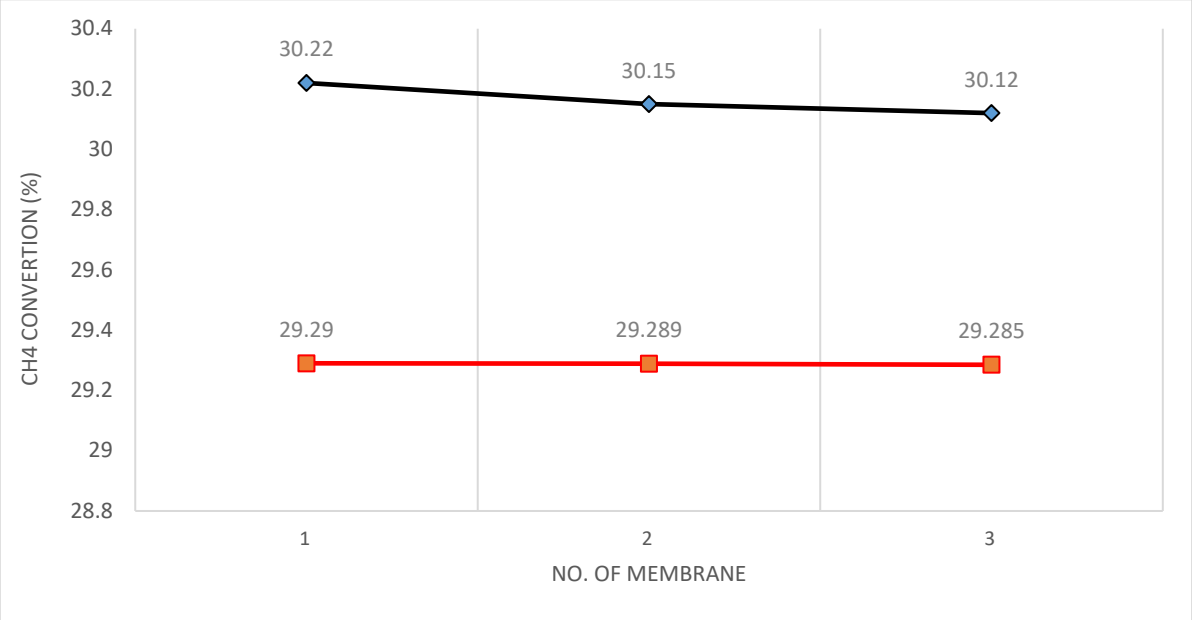

Figure 4. Comparison (Methane Conversion) of present work and previous work [20]

Figure 4 shows the simulated methane conversion compared with numerical work of (20). The comparison indicates a good agreement between the present work and the previous work with an error of less than 1% as appears in **Table 5**.

Table 6. Operation requirements

Description	Value
Inlet temperature, reformer bed, K	700–1000
Gas hourly space velocity, h^{-1}	1000
Carbon: Steam	1/3
Retentate Pressure, KPa	500 /400
Sweep gas Reynolds No.	100

Figure 6 illustrates the molar concentration of hydrogen (H_2) at a temperature of 1000 K in both the permeate and retentate sides. It is clearly observed that the H_2 concentration in the steam reforming zone is significantly higher than in the dry reforming zone.

This disparity can be attributed to two main factors:

1. The greater quantity of reforming products generated in the steam reforming reaction (reached to 42.1 mol/m^3) compared to the dry reforming reaction (0.133 mol/m^3).
2. The potential effect of the reverse water-gas shift (RWGS) reaction, which may reduce the net H_2 production in the dry reforming zone.

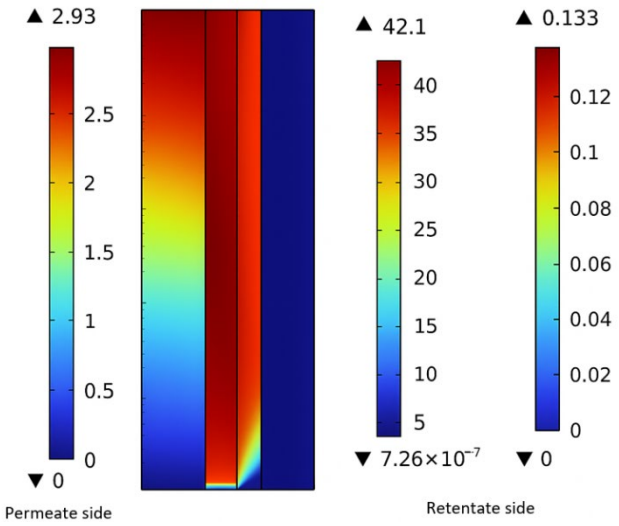

Figure 5. H_2 molar concentration

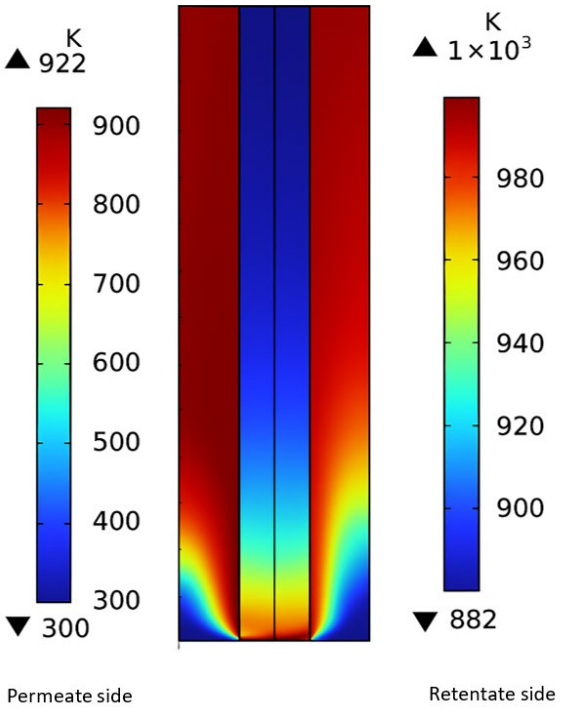

Figure 6. Temperature distribution

Figure 6 reveals that temperature profile at the retentate side achieves thermal homogeneity more rapidly than the permeate side, particularly under dry reforming conditions. This is likely due to the higher endothermic heat requirement of DRM reactions compared to SRM. The result emphasizes the importance of localized heat management and reactor design optimization in membrane reactors for hybrid reforming processes.

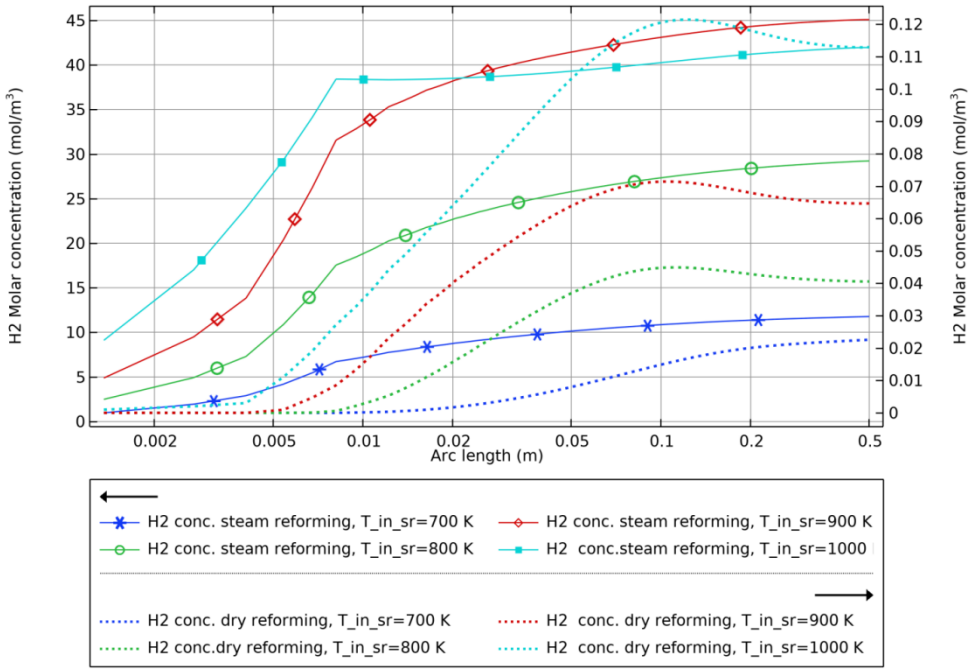

Figure 7. H_2 molar concentration in retentate of steam reforming side and dry reforming side

Figure 7 demonstrate that steam reforming contributes more significantly to hydrogen production in the retentate side compared to dry reforming. This is primarily due to the higher stoichiometric yield of hydrogen in the steam reforming reaction and its faster kinetics under similar conditions and also it depend on CO_2 permeance across the membrane to the dry reforming zone. Furthermore, increasing the inlet temperature enhances hydrogen production for both reactions, and the reactor length positively correlates with hydrogen mole fraction, especially at higher temperatures.

Although hydrogen mole concentration increases along the bed in the dry reforming section, a slight decrease or flattening is observed at the downstream end, particularly at high temperatures. This behavior may be attributed to the approach to chemical equilibrium, hydrogen consumption in secondary reactions such as the reverse water-gas shift, localized cooling effects, or depletion of methane and CO_2 reactants.

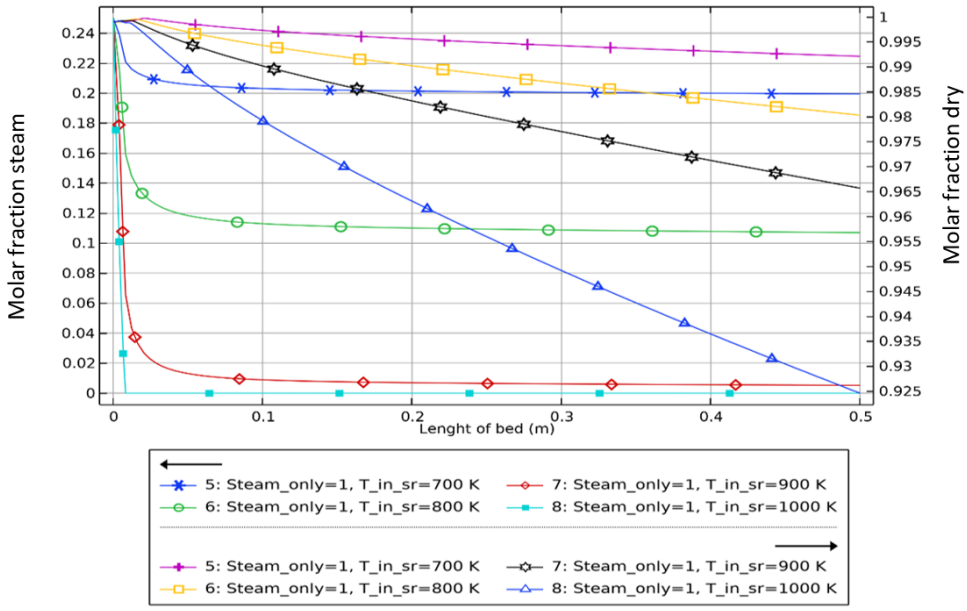

Figure 8. CH_4 molar fraction in steam reforming side and dry reforming side

Figure 8 presents the molar fraction profiles of methane (CH_4) along the hybrid reactor for different inlet temperatures in the steam reforming zone. The CH_4 molar fraction decreases sharply near the reactor inlet in the steam reforming section, indicating high conversion efficiency. This behavior is consistent with the known fast kinetics and strongly endothermic nature of the steam reforming reaction, which is favored at higher temperatures. As the inlet temperature increases from 700 K to 1000 K, the CH_4 depletion becomes more pronounced, reflecting a significant enhancement of the reaction rate with temperature. For instance, at 1000 K, CH_4 is almost completely consumed within the initial 0.05 m of the bed, whereas at 700 K, a considerable fraction remains.

In the downstream dry reforming zone, CH_4 concentrations are higher and decrease more gradually. This is due to the slower kinetics and less endothermic character of the dry reforming reaction compared to steam reforming. Despite the slower conversion, a continuous decrease in CH_4 along the reactor length is evident, confirming that CH_4 consumption persists in the dry reforming section.

Overall, increasing the inlet temperature in the steam reforming zone not only accelerates CH_4 conversion in that section but also contributes to higher CH_4 depletion in the dry reforming zone. This demonstrates the synergistic effect of the hybrid approach, where optimal temperature control in the steam reforming section enhances overall CH_4 conversion throughout the reactor.

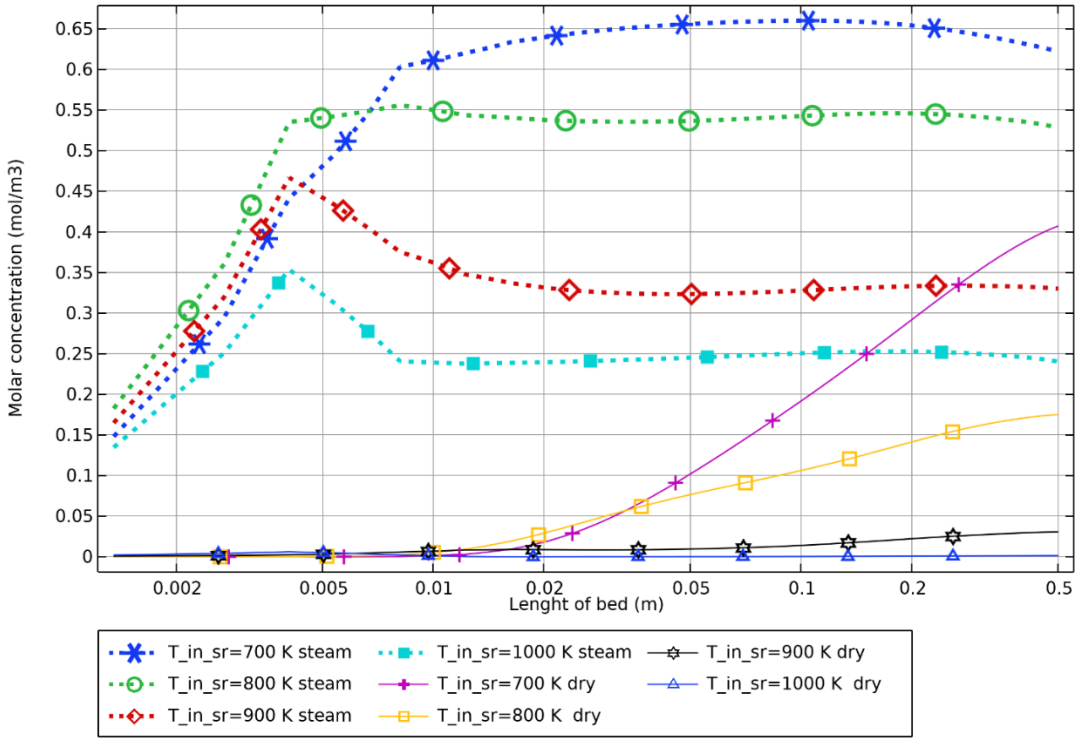

Figure 9(a). CO_2 molar concentration in steam reforming side and dry reforming side

Figure 9 (a) presents the molar concentration profile of CO_2 along the reactor bed in both the steam reforming and dry reforming zones at different inlet temperatures.

In the steam reforming side, CO_2 concentration generally decreases with increasing temperature, with the most effective consumption observed around 800 K, where reaction kinetics favor CO_2 conversion. At higher temperatures (900–1000 K), the concentration initially rises due to reaction dynamics but then stabilizes or decreases slightly along the reactor length. This pattern suggests that membrane permeation of CO_2 becomes significant at elevated temperatures, which can aid in shifting equilibrium and enhancing overall conversion.

On the dry reforming side, CO_2 concentration drops sharply and reaches nearly zero at 1000 K, indicating complete utilization. This is crucial to the design of hybrid reforming systems, as CO_2 consumption is a primary objective—not only to improve hydrogen yield, but also to utilize greenhouse gases, making the process environmentally sustainable. The system's effectiveness in removing CO_2 reflects its efficiency in coupling reaction and separation phenomena, which enhances conversion rates and drives the thermodynamic equilibrium forward.

Figure 9 (b) further emphasizes this by directly comparing CO_2 profiles at 1000 K, clearly showing the significant depletion of CO_2 on the dry reforming side, in contrast to the residual levels in steam reforming. This confirms that CO_2 conversion is maximized in the dry reforming zone, a key design outcome.

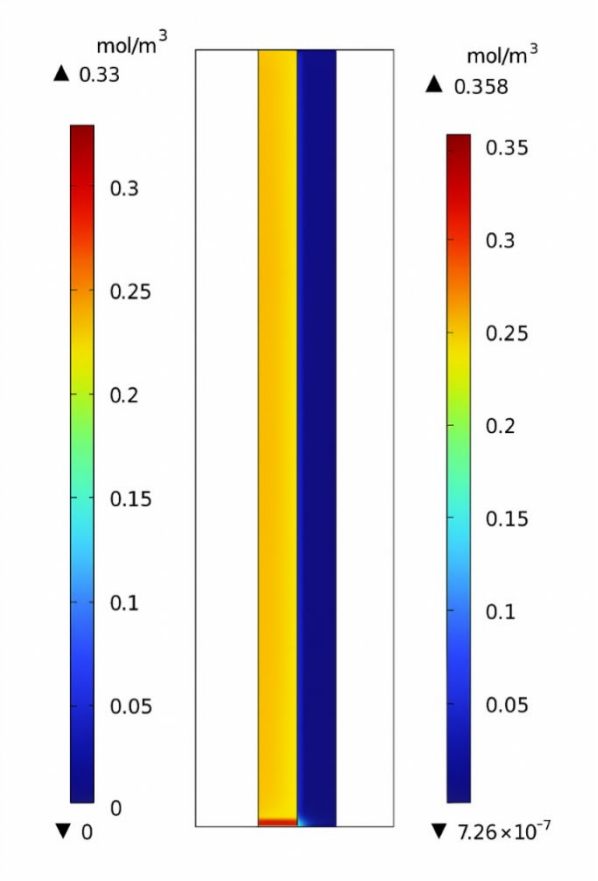

Figure 9(b). CO_2 molar concentration in steam reforming side and dry reforming side at 1000 K

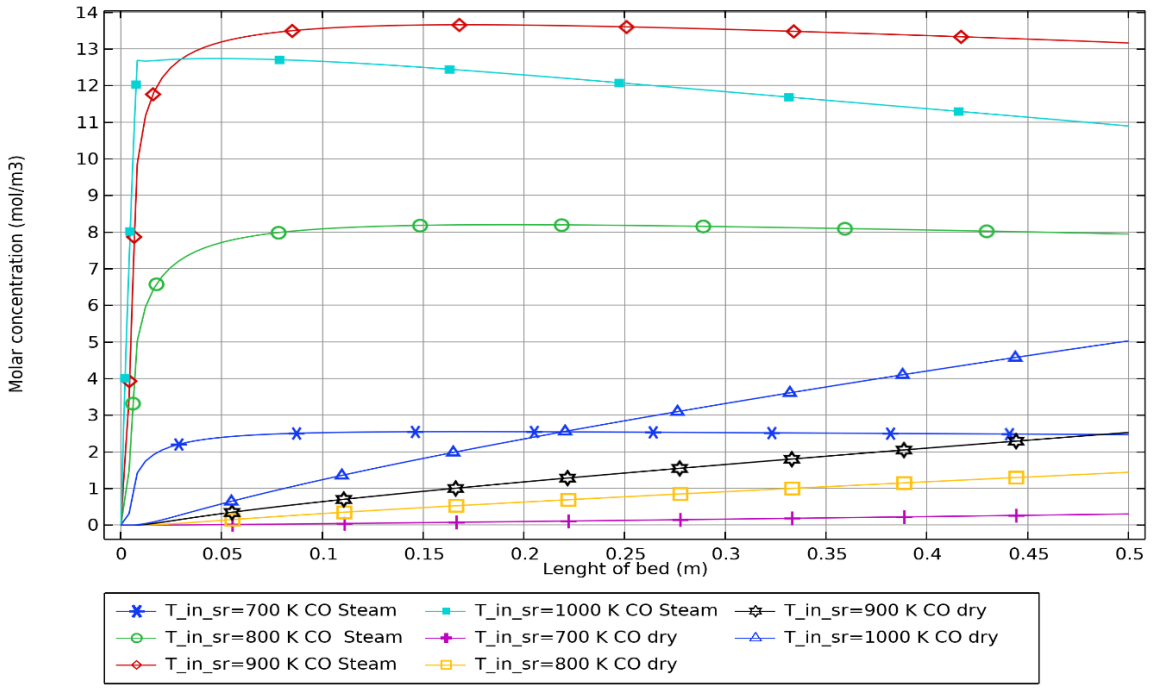

Figure 10. CO molar concentration

Figure 10 illustrates the molar concentration profile of carbon monoxide (CO) along the reactor bed in both the steam reforming and dry reforming zones at various inlet temperatures.

In the steam reforming side, as the temperature increases above 800 K, the CO molar concentration initially increases due to the primary steam reforming reaction:

$CH_4 + H_2O \rightarrow CO + 3H_2$

However, further along the reactor, the CO concentration begins to decrease, likely due to the water-gas shift reaction:

$CO + H_2O \rightarrow CO_2 + H_2$

This secondary reaction consumes CO, especially at higher H_2O concentrations and lower CO partial pressures. As a result, the CO profile reaches a peak at 900 K, which appears to be the temperature at which CO formation is maximized before significant shift conversion occurs.

In contrast, on the dry reforming side, the CO molar concentration consistently increases with temperature, due to the direct nature of the DRM reaction:

$CH_4 + CO_2 \rightarrow 2CO + 2H_2$

Since no significant CO-consuming side reactions occur here (like the water-gas shift), the CO formed remains largely in the system, leading to higher concentrations at elevated temperatures, especially at1000 K.

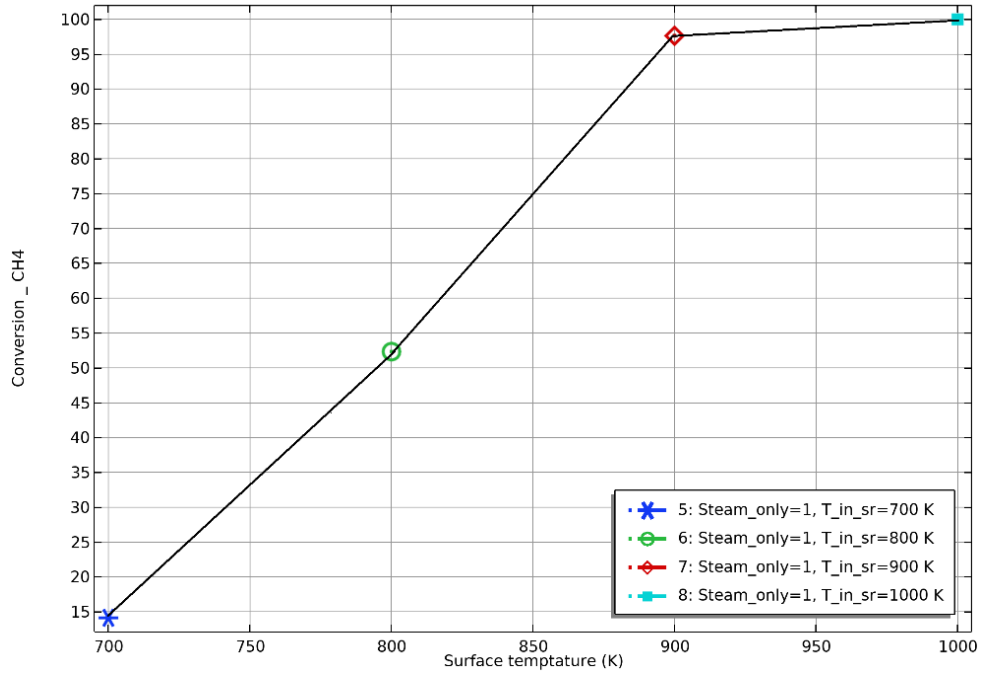

Figure 11(a). CH_4 conversion in steam reforming side

Figure 11 illustrates the CH_4 conversion on both the steam reforming(a) and dry reforming(b) sides. The conversion is significantly higher in the steam reforming zone, while it remains at an acceptable level in the dry reforming side, particularly when compared to the objective of CO_2 conversion. In both reforming zones, CH_4 conversion increases consistently with temperature, highlighting the thermal dependency of the reforming reactions.

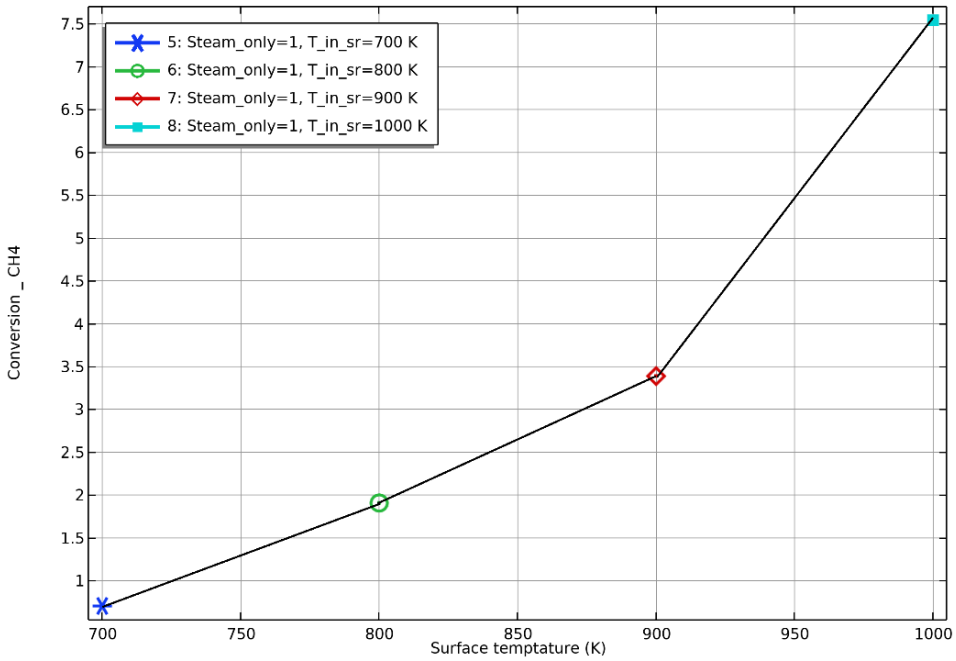

Figure 11(b). CH_4 conversion in dry reforming side

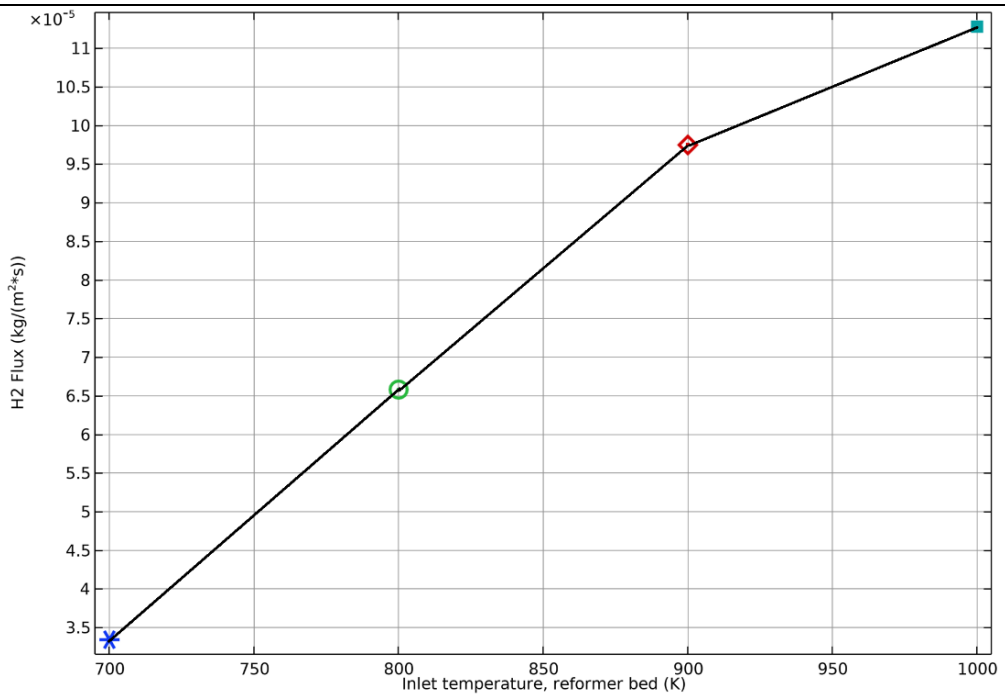

Figure 12. H_2 flux

Figure 12 demonstrate a clear positive correlation between the reformer bed inlet temperature and the hydrogen flux across the membrane. As the temperature increases from 700 K to 1000 K, the hydrogen flux rises from approximately 3.5×10^{-5} kg/m²·s to more than 1.1×10^{-4} kg/m²·s. This behavior can be attributed to the endothermic nature of the reforming reactions (steam reforming and dry reforming), which are thermodynamically favored at higher temperatures, leading to greater hydrogen production. In addition, the elevated temperature enhances the driving force for hydrogen permeation through the membrane due to the higher partial pressure of hydrogen on the reforming side.

It is evident that in the range of 800–900 K, the hydrogen flux increases sharply, indicating this interval as a highly favorable operating window for maximizing hydrogen recovery. Beyond 900 K, the flux continues to increase but with a reduced slope, suggesting that the system approaches equilibrium or experiences membrane transport limitations.

These findings highlight the critical role of temperature as a design parameter in hybrid reforming-membrane systems. While higher temperatures enhance hydrogen production, the diminishing returns observed at 1000 K emphasize the need to balance hydrogen yield against the additional energy input required for heating. Consequently, identifying the optimal operating temperature is essential to ensure both high efficiency and economic feasibility in industrial applications.

4. Conclusion

This study presents the development of a two-dimensional axisymmetric model of a hybrid catalytic membrane reactor designed to investigate the performance of a palladium-based catalytic membrane system for hydrogen production via the combined steam and dry reforming of natural gas (NG). The model was used to explore the effects of key operational parameters, including the use of argon as a sweep gas, reaction temperatures of 700 K, 800 K, 900 K, and 1000 K, a gas hourly space velocity (GHSV) of 1000 h^{-1}, and a Reynolds number (Re) of 100.

Based on the simulation results, the following conclusions were drawn:

- Reaction temperature was identified as the most influential factor affecting reactor performance. An increase in temperature led to a significant enhancement in CH_4 conversion, reaching up to 99.99% at 1000 K in the steam reforming zone. This also resulted in higher hydrogen production rates, primarily driven by improved hydrogen permeation through the palladium-based membrane.
- The novel reactor configuration proved effective in reducing CO_2 emissions from the steam reforming process by promoting its utilization in the dry reforming reaction. This not only contributed to increased hydrogen production but also improved carbon efficiency.
- The hybrid design significantly enhanced the overall syngas yield, which is a favorable outcome in terms of both energy efficiency and environmental sustainability. The system demonstrates clear potential for contributing to the reduction of global greenhouse gas emissions while optimizing hydrogen and syngas production processes.

Nomenclature

$\boldsymbol{\rho}_f$	Density fluid kg/m^3.
E	Catalytic bed void fraction.
X_i	Mass component fraction i.
M_i $D_{i,e}$	The i-component's molar mass and diffusion coefficient, respectively.
r_j	Reaction rate of j, kmol/m^3.s.
l	Thickness of membrane, m.
Pe_i	Coefficient of permeability, mol/s.m. pa$^{0.5}$.
$Pe_{o,i}$	Coefficient of constant.
$Ea_{,i}$	Activation energy of membrane, J/mol.
R	Constant of gas (8.314 kJ/kmol.K).
T	Temperature, K.
A	Cross-sectional area of reactor m^2.
➡ v	Velocity vector of the mixture gas.
ΔH_i	Heat of reaction or energy of adsorbed for surface species I, expressed in kJ/mol.
u	Velocity of gas, m/s.
P	Pressure total, bar.
M_i	Molecular weight of compound ith, g/mole.
Ci	Species concentration of i, kmol/m^3.
μ	Viscosity of gas, kg/m.s.
ρ_g	Gas Density, kg/m^3.
P_{cat}	Catalyst bed density, kg/m^3.
z	Coordinate axial m.
R_1	Radius of tube, m.
R_2	Radius of shell, m.

r_{cat}	Size of catalyst, mm
De	Coefficient effective of radial diffusion of component i m^2/s
κ	Permeability bed, m^2
D_{ij}	Diffusivity of binary gas, m^2/s
Q	Heat transfer kJ/s
k_{e1}, k_{e3}	Methane equilibrium constant reactions for steam reforming, pa^{-1}
k_{e2}	Methane equilibrium constant reaction for steam reforming
k_1,k_3	Methane kinetic-constant coefficients for steam reforming , kmol.pa $^{0.5}$/kg.s.
k_2	Methane kinetic-constant coefficient for steam reforming , kmol/pa.kg.s.
k_4	Methane kinetic-constant coefficient for dry reforming , kmol/kg.s.
k_5	Methane kinetic-constant coefficient for dry reforming , kmol/pa.kg.s.
KCH_4, KCO,KH_2, KCO_2	CH_4 CO, H_2,CO_2 constants of adsorption pa^{-1}
KH2O	H_2O constant adsorption
λij	Stoichiometric coefficient

Subscripts

GHSV	Gas Hourly Space Velocity.
CMR	Catalytic Membrane Reactor.
MSR	Methane Steam Reforming.
S	Shell side.
T	Tube side.
f	Fluid.
CFD	Computational Fluid Dynamics.
Pd	Palladium.
MR	Membrane Reactor.
SCR	Steam to Carbon Ratio.
NG	Natural Gas.

Conflict of interest

The authors declare no conflict of interest

References

1. Saimon, N. N., Jusoh, M., Kamarudin, M. J., Arsad, A., & Zakaria, Z. Y. (2017). Thermodynamic analysis of hydrogen production from methanol-ethanol-glycerol mixture through dry reforming. Chemical Engineering Transactions, 56, 967–972. https://doi.org/10.3303/CET1756162
2. Mazloomi, K., & Gomes, C. (2012). Hydrogen as an energy carrier: Prospects and challenges. In Renewable and Sustainable Energy Reviews (Vol. 16, Issue 5, pp. 3024–3033). https://doi.org/10.1016/j.rser.2012.02.028
3. Fang, X., Zhang, X., Guo, Y., Chen, M., Liu, W., Xu, X., Peng, H., Gao, Z., Wang, X., & Li, C. (2016). Highly active and stable Ni/Y2Zr2O7 catalysts for methane steam reforming: On the nature and effective preparation method of the pyrochlore support. International Journal of Hydrogen Energy, 41(26), 11141–11153. https://doi.org/10.1016/j.ijhydene.2016.04.038

4. Yurdakul, M., Ayas, N., Bizkarra, K., el Doukkali, M., & Cambra, J. F. (2016). Preparation of Ni-based catalysts to produce hydrogen from glycerol by steam reforming process. International Journal of Hydrogen Energy, 41(19), 8084–8091. https://doi.org/10.1016/j.ijhydene.2015.11.178
5. Kho, E. T., Scott, J., & Amal, R. (2016). Ni/TiO2 for low temperature steam reforming of methane. Chemical Engineering Science, 140, 161–170. https://doi.org/10.1016/j.ces.2015.10.021
6. Yang, X., Da, J., Yu, H., & Wang, H. (2016). Characterization and performance evaluation of Ni-based catalysts with Ce promoter for methane and hydrocarbons steam reforming process. Fuel, 179, 353–361. https://doi.org/10.1016/j.fuel.2016.03.104
7. Buelens, L. C., Galvita, V. V., Poelman, H., Detavernier, C., & Marin, G. B. (2016). Super-dry reforming of methane intensifies CO2 utilization via Le Chateliers principle. Science, 354(6311), 449–452. https://doi:10.1126/science.aah7161
8. le Saché, E., Pastor-Pérez, L., Watson, D., Sepúlveda-Escribano, A., & Reina, T. R. (2018). Ni stabilised on inorganic complex structures: superior catalysts for chemical CO2 recycling via dry reforming of methane. Applied Catalysis B: Environmental, 236, 458–465. https://doi.org/10.1016/j.apcatb.2018.05.051
9. Pappacena, A., Razzaq, R., de Leitenburg, C., Boaro, M., & Trovarelli, A. (2018). The role of neodymium in the optimization of a Ni/CeO2 and Ni/CeZrO2 Methane dry reforming catalyst. Inorganics, 6(2). https://doi.org/10.3390/inorganics6020039
10. Littlewood, P., Xie, X., Bernicke, M., Thomas, A., & Schomäcker, R. (2015). Ni0.05Mn0.95O catalysts for the dry reforming of methane. Catalysis Today, 242(Part A), 111–118. https://doi.org/10.1016/j.cattod.2014.07.054
11. Chen, L., Gangadharan, P., & Lou, H. H. (2018). Sustainability assessment of combined steam and dry reforming versus tri-reforming of methane for syngas production. Asia-Pacific Journal of Chemical Engineering, 13(2). https://doi.org/10.1002/apj.2168
12. Behroozsarand, A., & Pour, A. N. (2014). Modeling of microreactor for methane dry reforming: Comparison of Langmuir-Hinshelwood kinetic and microkinetic models. Journal of Natural Gas Science and Engineering, 20, 99–108. https://doi.org/10.1016/j.jngse.2014.06.011
13. Kassi, A. H., & Al-Hattab, T. A. (2024). A CFD model of natural gas steam reforming in a catalytic membrane reactor: Effect of various operating parameters on the performance of CMR. International Journal of Hydrogen Energy, 56, 780–796. https://doi.org/10.1016/j.ijhydene.2023.12.156
14. Fedotov, A. S., Antonov, D. O., Uvarov, V. I., & Tsodikov, M. v. (2018). Original hybrid membrane-catalytic reactor for the Co-Production of syngas and ultrapure hydrogen in the processes of dry and steam reforming of methane, ethanol and DME. International Journal of Hydrogen Energy, 43(14), 7046–7054. https://doi.org/10.1016/j.ijhydene.2018.02.060
15. Tosti, S., Borgognoni, F., & Santucci, A. (2010). Multi-tube Pd-Ag membrane reactor for pure hydrogen production. International Journal of Hydrogen Energy, 35(20), 11470–11477. https://doi.org/10.1016/j.ijhydene.2010.06.102
16. Basile, A., Iulianelli, A., Longo, T., Liguori, S., & de Falco, M. (2011). Pd-based Selective Membrane State-of-the-Art. In Membrane Reactors for Hydrogen Production Processes (pp. 21–55). Springer London. https://doi.org/10.1007/978-0-85729-151-6_2
17. Lee, S., & Lim, H. (2020). Utilization of CO2 arising from methane steam reforming reaction: Use of CO2 membrane and heterotic reactors. Journal of Industrial and Engineering Chemistry, 91, 201–212. https://doi.org/10.1016/j.jiec.2020.08.001
18. Chen, T., Yu, B., Zhao, Y., Li, Y., & Lin, Y. S. (2017). Carbon dioxide permeation through ceramic-carbonate dual-phase membrane-effects of sulfur dioxide. Journal of Membrane Science, 540, 477–484. https://doi.org/10.1016/j.memsci.2017.06.063
19. Richardson, J. T., & Paripatyadar, S. A. (1990). Carbon Dioxide Reforming of Methane with Supported Rhodium. In Applied Catalysis. Elsevier Science Publishers B.V.
20. Lee, S., & Lim, H. (2020). The effect of changing the number of membranes in methane carbon dioxide reforming: A CFD study. Journal of Industrial and Engineering Chemistry, 87, 110–119. https://doi.org/10.1016/j.jiec.2020.03.020.
21. Lim, Y., Lee, C. J., Jeong, Y. S., Song, I. H., Lee, C. J., & Han, C. (2012). Optimal design and decision for combined steam reforming process with dry methane reforming to reuse CO 2 as a raw material. Industrial and Engineering Chemistry Research, 51(13), 4982–4989. https://doi.org/10.1021/ie200870m
22. Xu, J., & Froment, G. F. (1989). Methane steam reforming, methanation and water-gas shift: I. Intrinsic kinetics. AIChE journal, 35(1), 88-96.
23. Anzelmo, B., Wilcox, J., & Liguori, S. (2018). Hydrogen production via natural gas steam reforming in a Pd-Au membrane reactor. Comparison between methane and natural gas steam reforming reactions. Journal of Membrane Science, 568, 113–120. https://doi.org/10.1016/j.memsci.2018.09.054
24. Chompupun, T., Limtrakul, S., Vatanatham, T., Kanhari, C., & Ramachandran, P. A. (2018). Experiments, modeling and scaling-up of membrane reactors for hydrogen production via steam methane reforming. Chemical Engineering and Processing - Process Intensification, 134, 124–140. https://doi.org/10.1016/j.cep.2018.10.007

25. Nayebossadri, S., Speight, J. D., & Book, D. (2019). Hydrogen separation from blended natural gas and hydrogen by Pd-based membranes. International Journal of Hydrogen Energy, 44(55), 29092–29099. https://doi.org/10.1016/j.ijhydene.2019.03.044
26. Gangadharan, P., Kanchi, K. C., & Lou, H. H. (2012). Evaluation of the economic and environmental impact of combining dry reforming with steam reforming of methane. Chemical Engineering Research and Design, 90(11), 1956–1968. https://doi.org/10.1016/j.cherd.2012.04.008
27. Lee, J., Kim, B., & Han, M. (2019). Spatially Patterned Catalytic Reactor for Steam-CO2 Reforming of Methane. Industrial and Engineering Chemistry Research, 58(40), 18731–18741. https://doi.org/10.1021/acs.iecr.9b03091
28. Ullah, K. S., Omer, A., Rashid, K., Rehman ,N. U., Rahimipetroudi, I., Kim, S. D., & Dong, S. K. (2023). Modeling and comprehensive analysis of hydrogen production in a newly designed steam methane reformer with membrane system. Computers & Chemical Engineering, 175, 108278
29. Su, B., Wang, Y., Xu, Z., Han, W., Jin, H., & Wang, H. (2022). Novel ways for hydrogen production based on methane steam and dry reforming integrated with carbon capture. Energy Conversion and Management, 270. https://doi.org/10.1016/j.enconman.2022.116199
30. Jabbour, K. (2020). Tuning combined steam and dry reforming of methane for "metgas" production: A thermodynamic approach and state-of-the-art catalysts. In Journal of Energy Chemistry (Vol. 48, pp. 54–91). Elsevier B.V. https://doi.org/10.1016/j.jechem.2019.12.017
31. Shakouri, M., Hu, Y., Lehoux, R., & Wang, H. (2021). CO2 conversion through combined steam and CO2 reforming of methane reactions over Ni and Co catalysts. Canadian Journal of Chemical Engineering, 99(1), 153–165. https://doi.org/10.1002/cjce.23828
32. Ghasem, N. (2022). A Review of the CFD Modeling of Hydrogen Production in Catalytic Steam Reforming Reactors. In International Journal of Molecular Sciences (Vol. 23, Issue 24). MDPI. https://doi.org/10.3390/ijms232416064